

BEST AVAILABLE COPY

Los Alamos National Laboratory

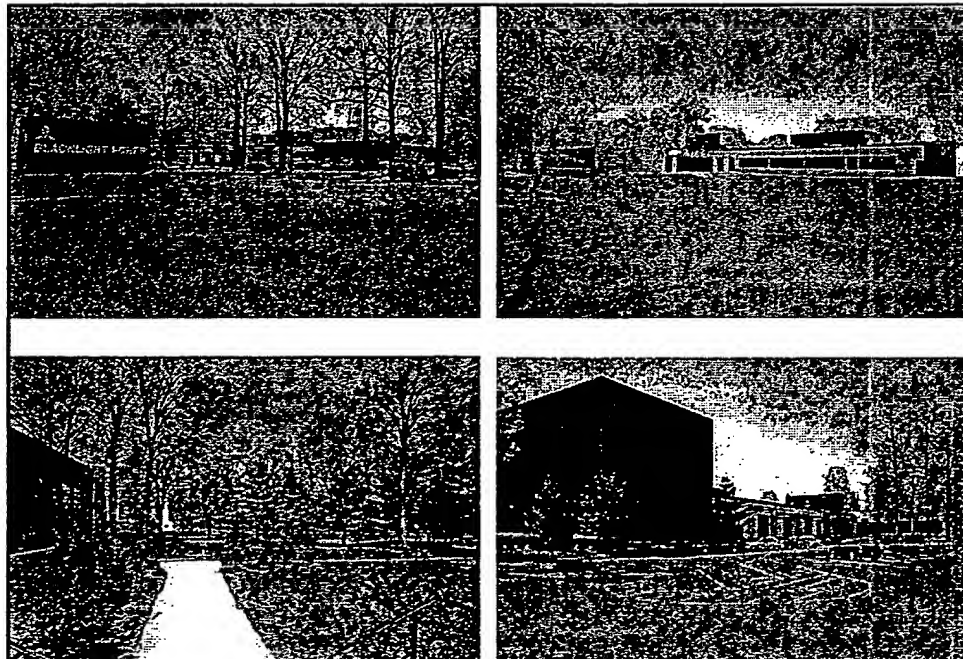
November 25, 2002

Los Alamos, NM

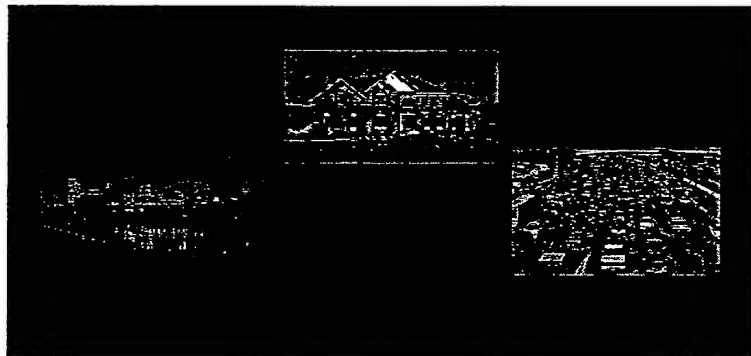
Novel Catalytic Reaction of Hydrogen as a Potential New Energy Source

Randell Mills, Xuemin Chen, Bala Dhandapani,
William Good, Jiliang He, Robert Mayo, Mark Nansteel,
Paresh Ray, Jayasree Sankar, Andreas Voigt

BlackLight Power, Inc.
493 Old Trenton Road, Cranbury, NJ 08512



Breakthrough in Hydrogen Chemistry with Paradigm-Shifting Applications



Hydrogen Catalysts

From a solution of a Schrödinger-type wave equation with a nonradiative boundary condition based on Maxwell's equations, atomic hydrogen may undergo a catalytic reaction with certain atomized elements such as potassium, cesium, and strontium atoms or certain gaseous ions such as Ar^+ which singly or multiply ionize at integer multiples of the potential energy of atomic hydrogen, 27.2 eV. The reaction involves a nonradiative energy transfer to form an increased binding energy hydrogen atom called a hydrino having a binding energy of

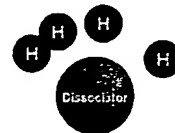
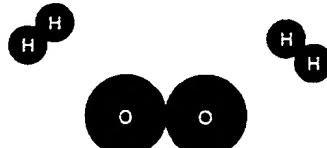
$$\text{Binding Energy} = \frac{13.6 \text{ eV}}{\left(\frac{1}{p}\right)^2}$$

where p is an integer greater than 1, designated as $H\left[\frac{a_H}{p}\right]$ where a_H is a radius of the hydrogen atom. Hydrinos are predicted to form by reacting an ordinary hydrogen atom with a catalyst having a net enthalpy of reaction of about $m \cdot 27.2 \text{ eV}$, where m is an integer. This catalysis releases energy from the hydrogen atom with a commensurate decrease in size of the hydrogen atom, $r_h = n a_H$.

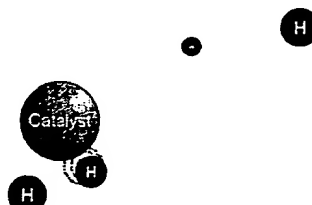
For example, the catalysis of $H(n=1)$ to $H(n=1/2)$ releases 40.8 eV, and the hydrogen radius decreases from a_H to $\frac{1}{2} a_H$.

Step 1: Water is broken down to hydrogen and oxygen molecules through electrolysis.

Step 2: Oxygen is released and a dissociator is added to split each hydrogen molecule into two hydrogen atoms. Alternatively a plasma causes dissociation



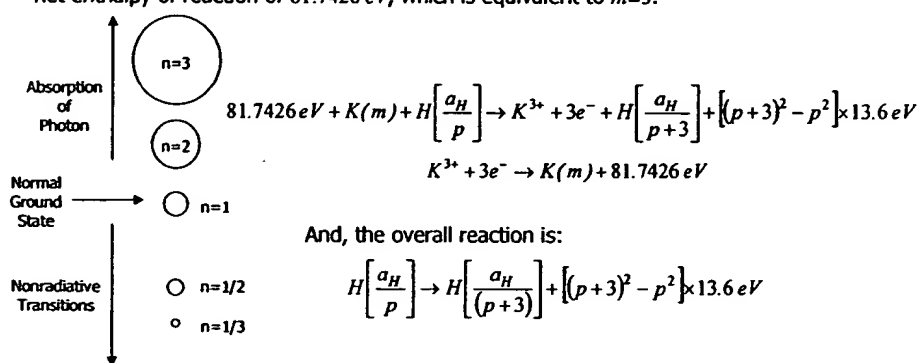
Step 3: A catalyst reacts with atomic hydrogen releases substantial energy, forms hydrides, and creates or greatly intensifies a plasma that is extremely energetic or hot.



The Theory Allows Energy to be Extracted from a Hydrogen Atom

Hydrogen electrons are stimulated to a fractional quantum state by the presence of a catalyst with a net enthalpy of reaction of $m \cdot 27.2 \text{ eV}$.

A catalytic system is provided by the ionization of i electrons from an atom each to a continuum energy level such that the sum of the ionization energies of the i electrons is approximately $m \cdot 27.2 \text{ eV}$, where m is an integer. One such catalytic system involves potassium. The first, second, and third ionization energies of potassium are 4.34066 eV , 31.63 eV , 45.806 eV respectively. The triple ionization ($i=3$) reaction of K to K^{3+} , then, has a net enthalpy of reaction of 81.7426 eV , which is equivalent to $m=3$.



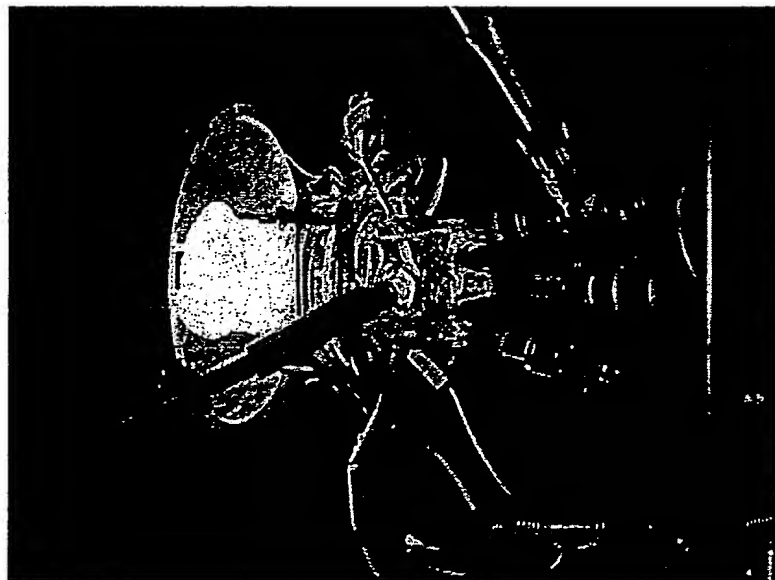
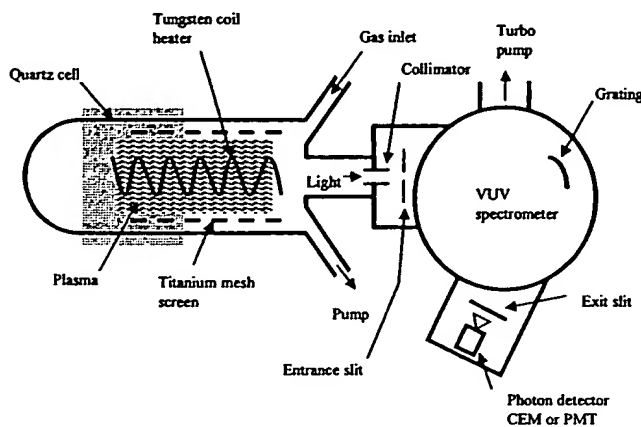
Catalyst Resonant Energy Transfer

- $K(m) + 81.742 \text{ eV} (3 \times 27.2 \text{ eV}) \rightarrow K^{3+} + 3e^-$
- $K^+ + K^+ + 27.2 \text{ eV} \rightarrow K^{2+} + K$
- $Rb^+ + 27.28 \text{ eV} \rightarrow Rb^{2+} + e^-$
- $Sr^+ + 54.4 \text{ eV} (2 \times 27.2 \text{ eV}) \rightarrow Sr^{3+} + 2e^-$
- $He^+ + 54.4 \text{ eV} (2 \times 27.2 \text{ eV}) \rightarrow He^{2+} + e^-$
- $Ar^+ + 27.2 \text{ eV} \rightarrow Ar^{2+} + e^-$
- $O_2 + 54.4 \text{ eV} (2 \times 27.2 \text{ eV}) \rightarrow O^{2+} + O + 2e^-$

Based on H Catalyst Reaction

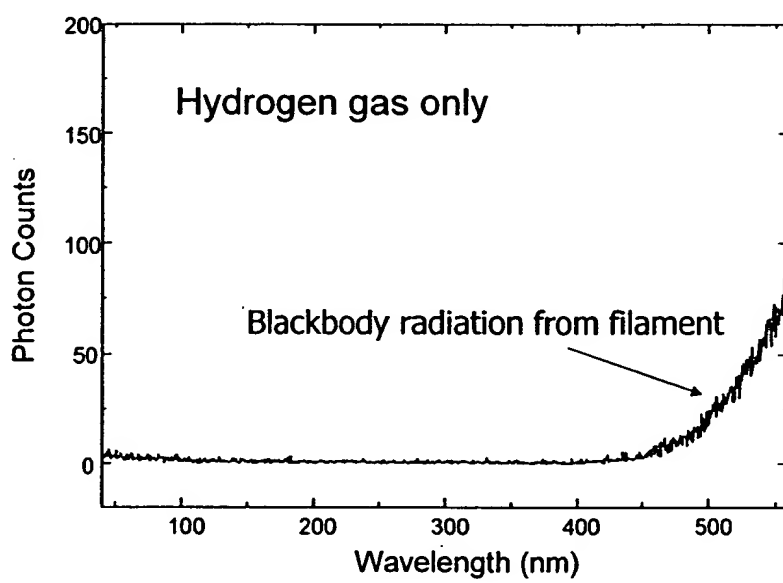
- Chemically Generated or Assisted Plasmas
- Lower-Energy Hydrogen Emission and Isolation
- Catalyst Emission
- Line Broadening
- Thermal and Optical Power
- Balmer and Lyman Line Inversions
- Novel Chemical Compounds
- Novel Processes

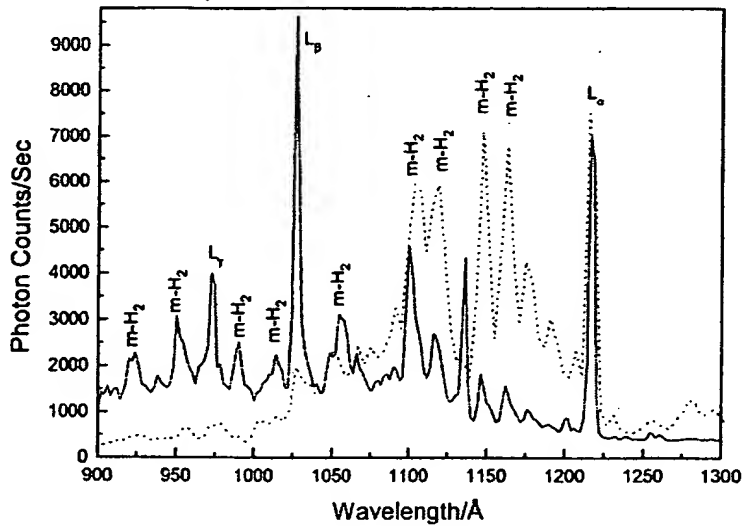
Experimental Set-up for Chemically-Generated RT Plasma



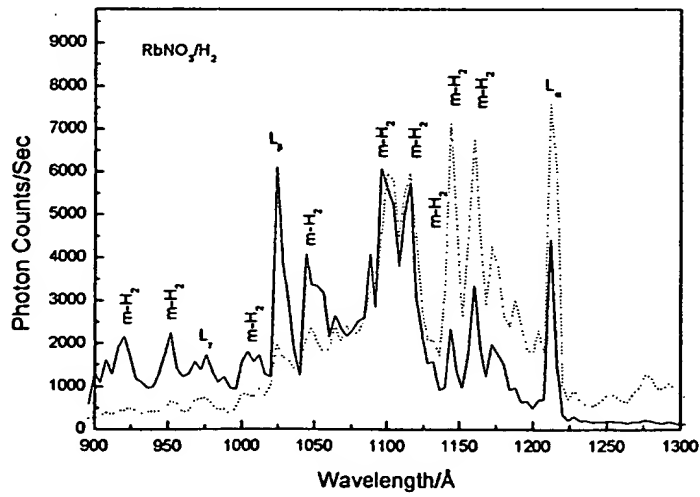
Hydrogen Catalyst Reaction Products

- Plasma
- Light
- Power
- Novel Hydrogen Compounds

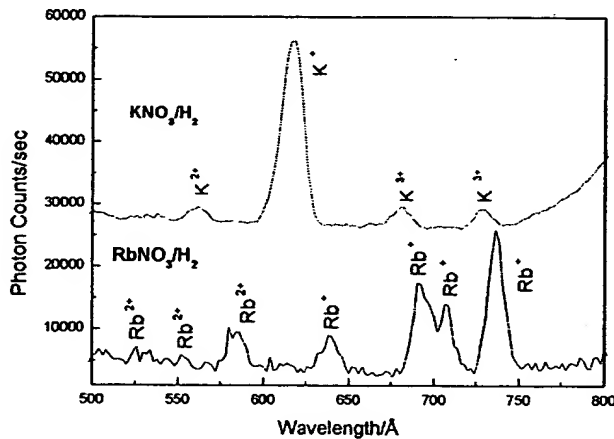




The VUV spectra (900–1300 Å) of the cell emission from hydrogen microwave plasma (dotted line) and the KNO_3 – H_2 rt-plasma (solid line) with an inverted Lyman population.

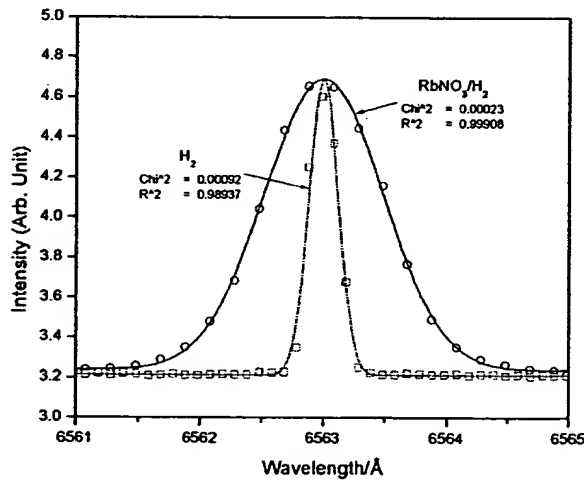


The VUV spectra (900–1300 Å) of the cell emission from hydrogen microwave plasma (dotted line) and the $RbNO_3$ - H_2 rt-plasma (solid line) with an inverted Lyman population.

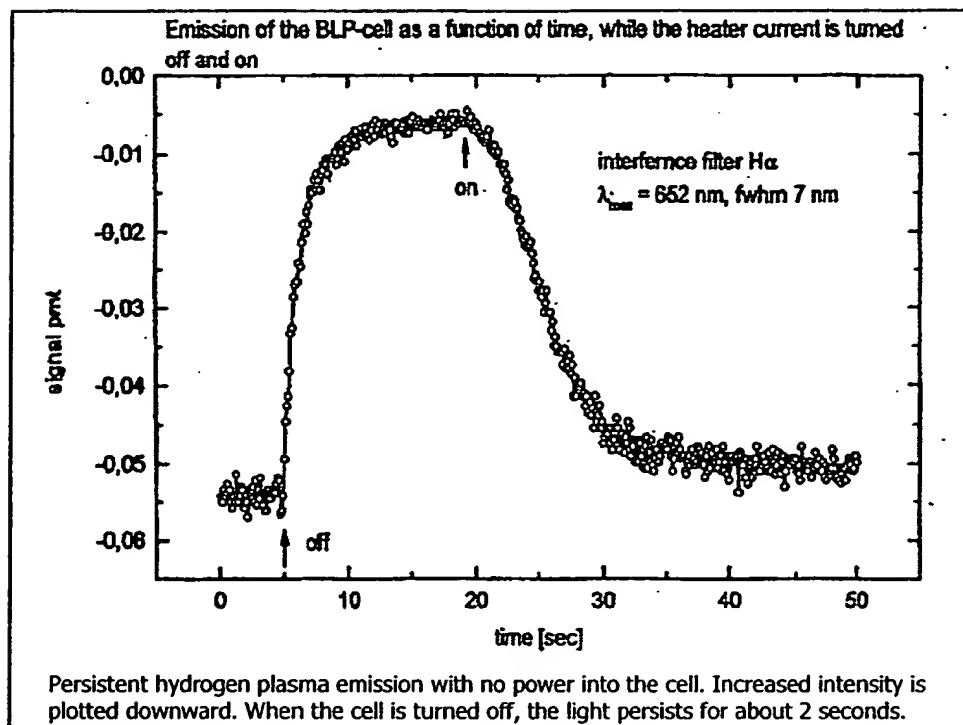


The VUV spectrum (500–800 Å) of the emission of the $\text{KNO}_3\text{-H}_2$ gas cell (top curve) and the $\text{RbNO}_3\text{-H}_2$ gas cell (bottom curve). The gas cell comprised a tungsten filament, a titanium dissociator, 300 mTorr hydrogen, and vaporized K^+ or Rb^+ from KNO_3 or RbNO_3 , respectively. The emission was recorded with a CEM at a cell temperature of 700 °C. Line emission corresponding to K^{2+} was observed at 553 Å, and K^+ was observed at 620 Å. K^{3+} was observed at 672 Å and 737 Å. Line emission corresponding to Rb^{2+} was observed at 533 Å, 556 Å, and 581 Å. Rb^+ was observed at 643 Å, 697 Å, 711 Å, and 741.5 Å.

Balmer α Line Broadening

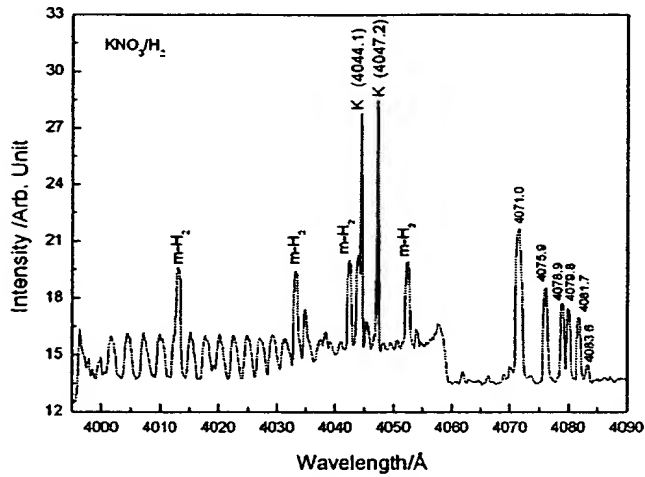


Significant broadening of Balmer α line was observed corresponding to an average hydrogen atom temperature of 10–14 eV compared to that of a microwave hydrogen plasma of 1–2 eV.

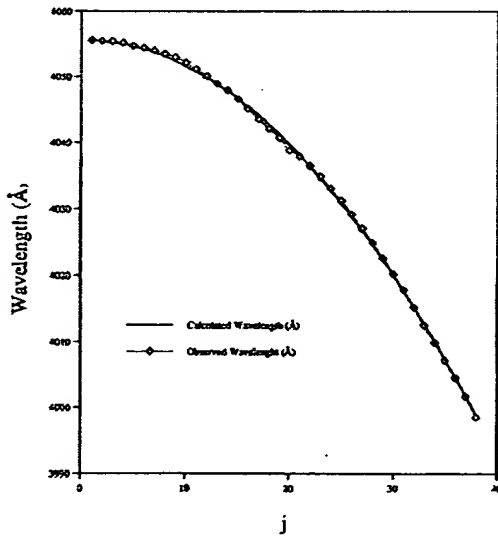


Spectral Emission of Fractional- Principal-Quantum-Energy-Level Hydride Ion

OBSERVED
 with a
 High Resolution Visible
 Spectrometer



The binding energy emission of H⁻(1/2) hydride ion formed with K⁺ catalyst at 4071 Å with the predicted inverse Rydberg series of hyperfine lines with energies E_{HF} given by
 $E_{HF} = j^2 3.00213 \times 10^{-5} + 3.0563 \text{ eV}$ for $j=1$ to $j=38$.

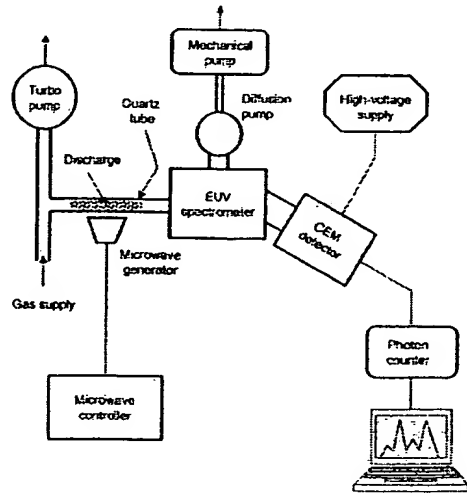


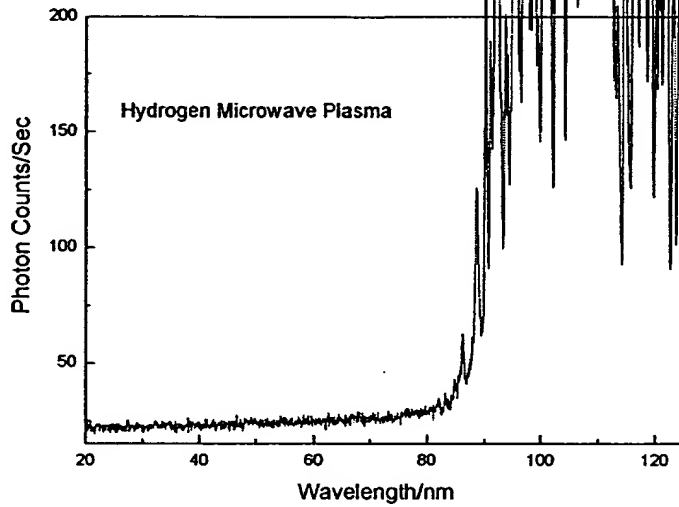
The plot of the theoretical bound-free hyperfine air wavelengths corresponding to energies E_{HF} given by $E_{HF} = j^2 3.00213 \times 10^{-5} + 3.0563 \text{ eV}$ for $j=1$ to $j=38$ and the wavelengths observed for the inverse Rydberg-type series of broad emission lines.

Spectral Emission of Fractional- Principal-Quantum-Energy-Level Atomic Hydrogen

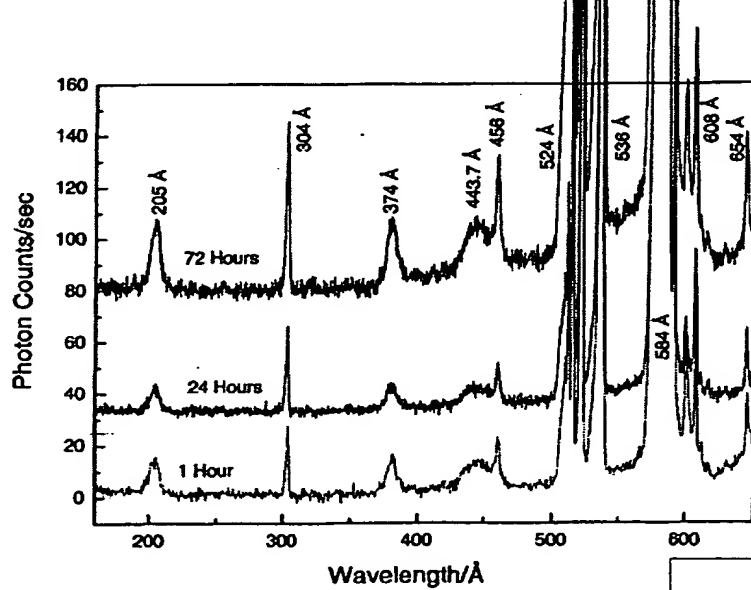
OBSERVED
with a
Normal Incidence EUV
Spectrometer

BLP Microwave Discharge Light Source

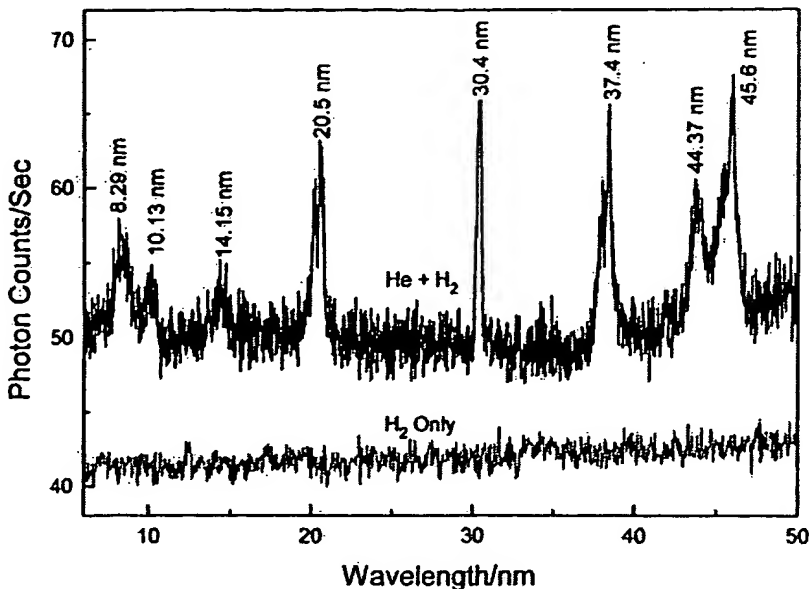




Hydrogen spectrum with no emission for $\lambda < 800 \text{ \AA}$.



Helium/hydrogen plasma shows hydrino emission peaks.



Hydrino emission peaks at short wavelenghts.

The Novel Lines can be Explained as Electronic Transitions to Fractional Rydberg States of Atomic Hydrogen

- Electronic transitions to fractional Rydberg states given by

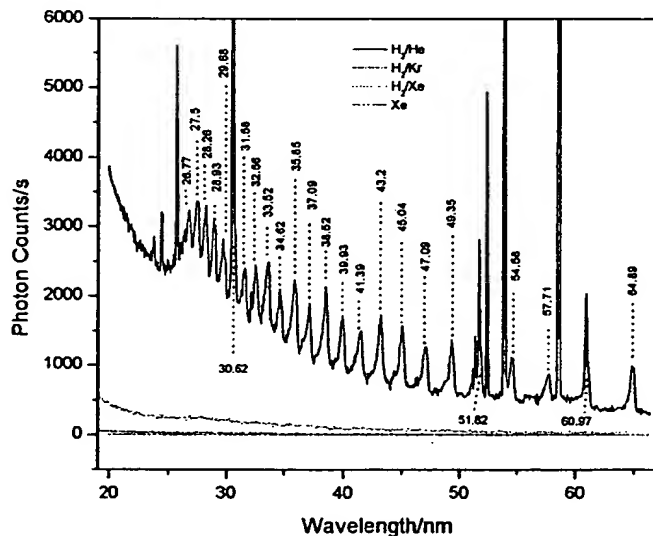
$$E_n = -\frac{e^2}{n^2 8\pi \epsilon_0 a_H} = \frac{13.598 \text{ eV}}{n^2} \quad n = \frac{1}{2}, \frac{1}{3}, \frac{1}{4}, \dots, \frac{1}{p};$$

p is an integer catalyzed by the resonant nonradiative transfer of $m \cdot 27.2 \text{ eV}$ would give rise to a series of emission lines of energies $q \cdot 13.6 \text{ eV}$ where q is an integer.

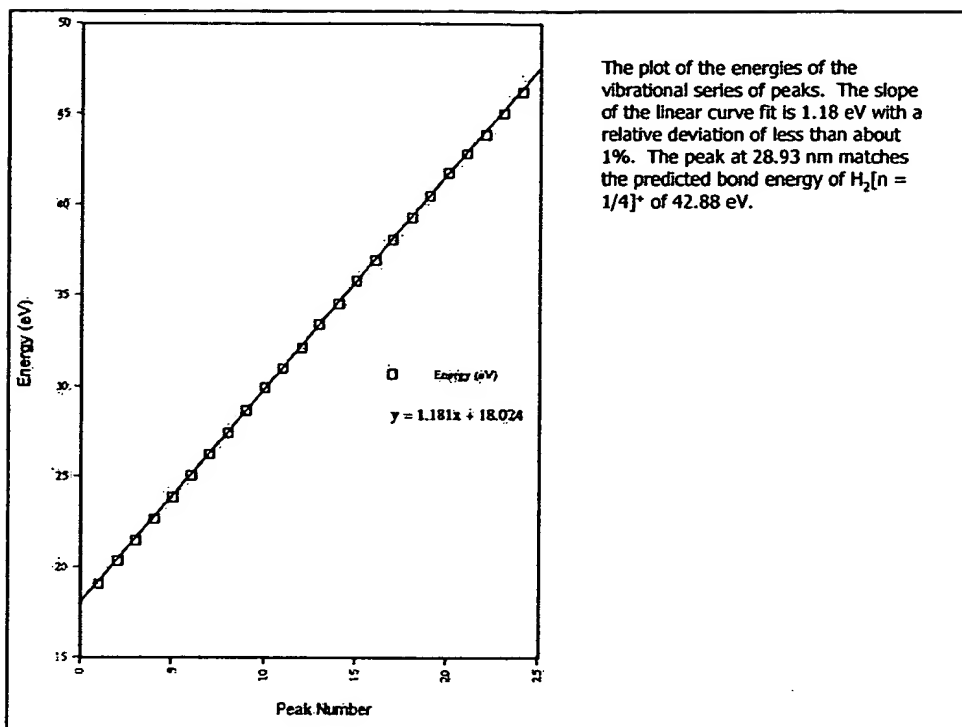
- Novel EUV emission lines with energies of $q \cdot 13.6 \text{ eV}$ where $q=1, 2, 3, 4, 6, 7, 8, 9, \text{ or } 11$ or these lines inelastically scattered by helium atoms in the excitation of $\text{He}(1s^2)$ to $\text{He}(1s^1 2p^1)$ matched hydrogen transitions to electronic energy levels below the "ground" state corresponding to fractional quantum numbers

Vibrational Spectral Emission of Fractional-Principal-Quantum-Energy-Level Hydrogen Molecular Ion

Observed
with a
4 ° Grazing Incidence EUV
Spectrometer

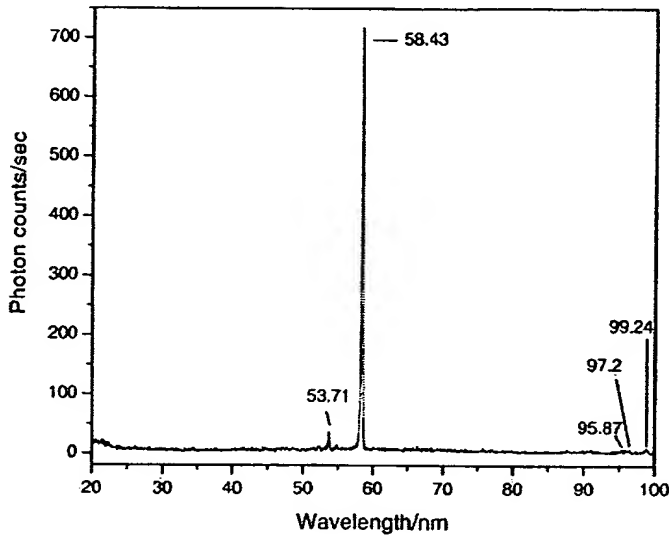


In the EUV spectrum (20–65 nm), a vibrational pattern of peaks with an energy spacing of 1.18 eV was observed from the helium-hydrogen (90/10%) microwave plasma having He⁺ catalyst. The peak at 28.93 nm matched the predicted bond energy of H₂[n = 1/4]^{*} of 42.88 eV. No emission was observed from the krypton and xenon controls.

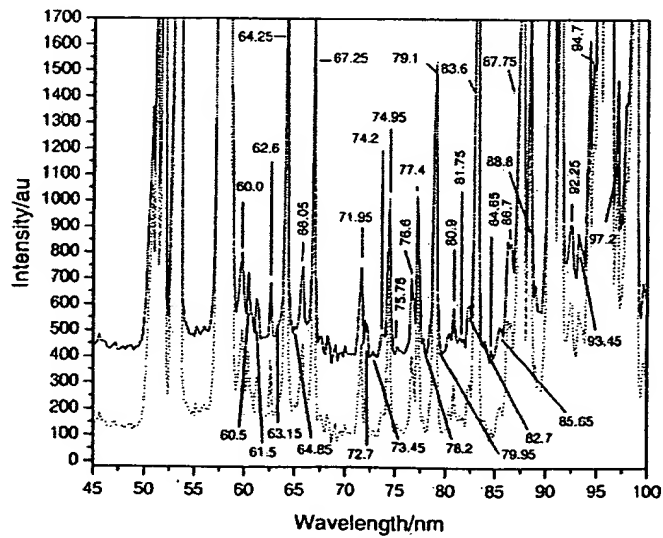


Spectral Emission of Fractional- Principal-Quantum-Energy-Level Molecule

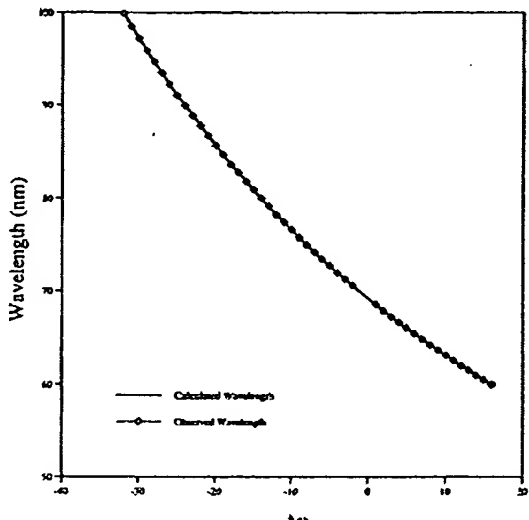
OBSERVED
with a
High Resolution Visible
Spectrometer



The EUV spectrum (20-100 nm) of the control helium microwave discharge cell emission at 1 Torr that was recorded with a normal incidence EUV spectrometer and a CEM. Only known He I and He II peaks were observed.



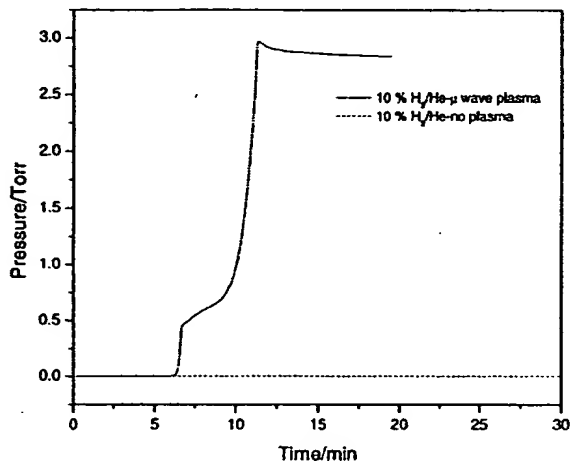
Two EUV spectra (45-100 nm) of the microwave cell emission of the helium-hydrogen (98/2%) plasma that showed peaks that matched those predicted at $E_{D+vb} = p^2 E_{DH_2} \pm \left(\frac{\nu^*}{3}\right) E_{vb H_2(\nu=0 \rightarrow \nu=1)}$ due to the reaction $2H(1/2) \rightarrow H_2(1/2)$ with vibronic coupling. The series of peaks due to vibronic coupling is centered about the bond energy of 17.913 eV.



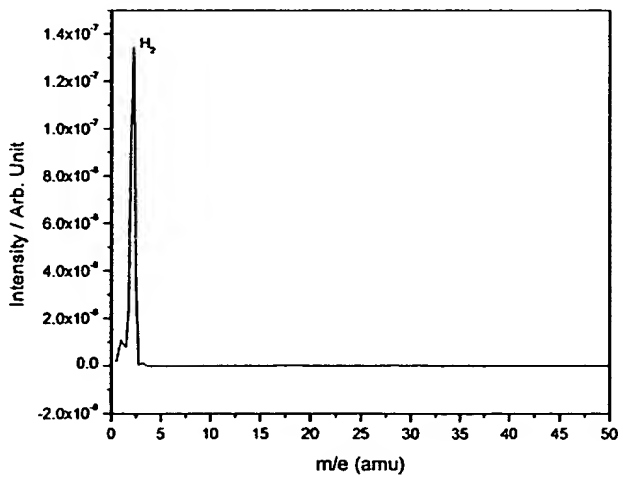
The EUV plasma emission spectra in the region 60 nm to 100 nm matched the predicted emission lines E_{D+H_2} due to the reaction $2H(1/2) \rightarrow H_2(1/2)$ with vibronic coupling at energies of $E_{D+rib} = p^2 E_{D,H_2} \pm \left(\frac{\nu^*}{3}\right) E_{rib, H_2(\nu=0 \rightarrow \nu=1)}$ ($p=2$) to longer wavelengths for $\nu^*=2$ to $\nu^*=32$ and to shorter wavelengths for $\nu^*=1$ to $\nu^*=16$ to within the spectrometer resolution of $\pm 0.05\%$.

Isolation of Fractional-Principal-Quantum-Energy-Level Molecular Hydrogen

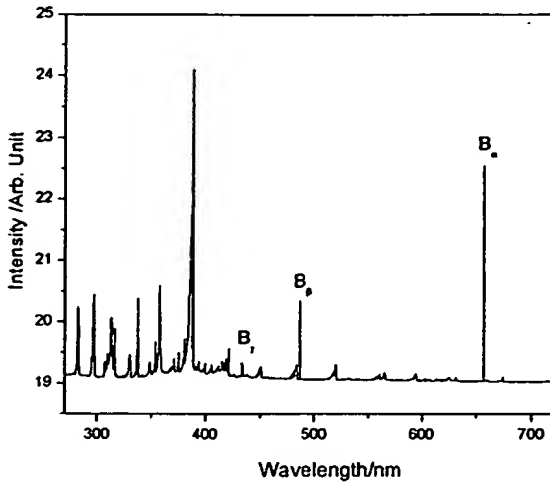
by Condensation at Liquid Nitrogen Temperature



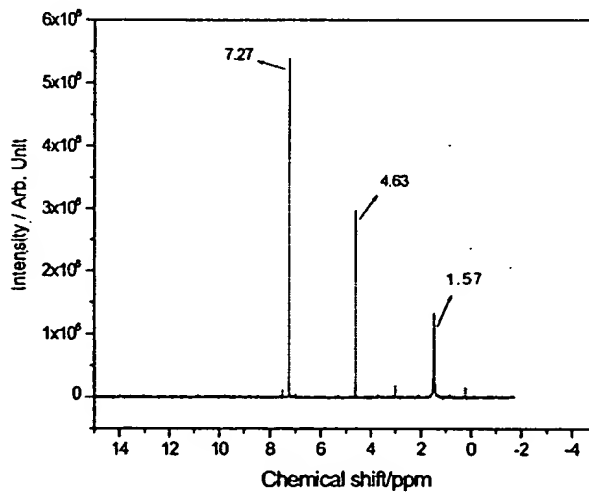
The pressure as a function of time after the liquid nitrogen dewar was removed from the U-tube cryotrap following 2 hours of helium-hydrogen (90/10%) gas flow through the microwave tube and the cryosystem without plasma (dotted) and with a plasma maintained with 60 W forward microwave power and 10 W reflected (solid). A liquid-nitrogen condensable gas product was only observed for the plasma reaction run.



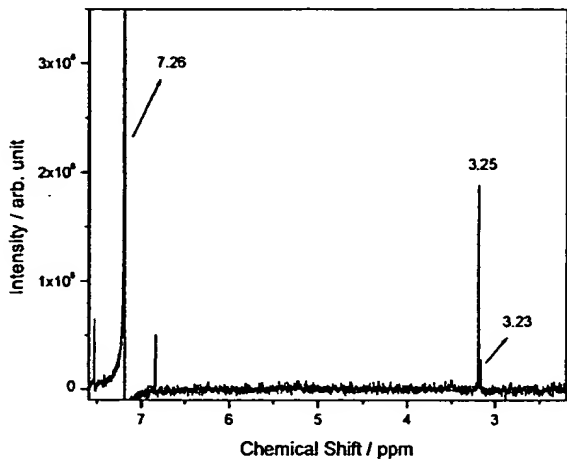
The mass spectrum (m/e = 1 to m/e = 50) of the condensed gas from the helium-hydrogen (90/10%) plasma run for 2 hours. Only hydrogen peaks were observed which identified the liquid-nitrogen-condensable gas as hydrogen.



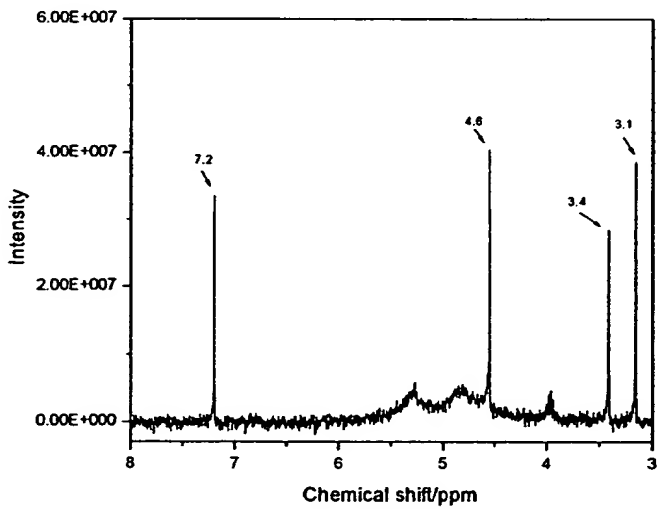
The high resolution (± 0.1 nm) visible optical emission spectrum (275–725 nm) recorded on a microwave discharge plasma of the liquid-nitrogen-condensable helium-hydrogen (90/10%) microwave discharge plasma gas. Strong Balmer α , β , γ and δ lines of atomic hydrogen were observed at 656.28 nm, 486.13 nm, 434.05 nm, and 410.17 nm, respectively, which indicated that the gas contained hydrogen. The spectrum did not match that of any known gas.



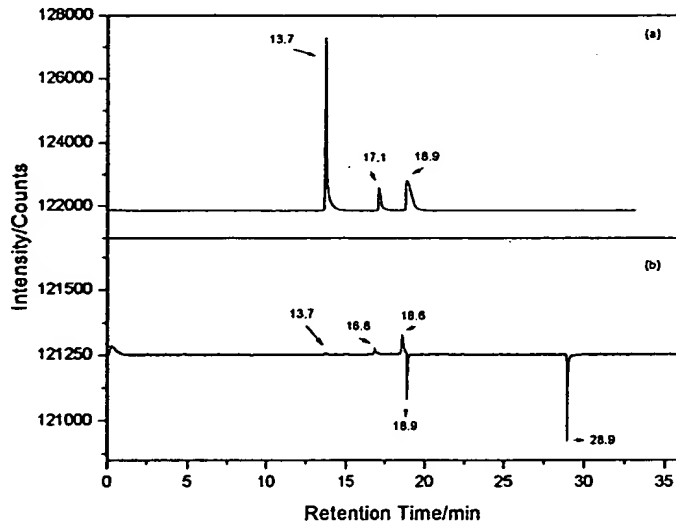
The ^1H NMR spectrum on a sealed sample of ultrahigh purity hydrogen dissolved in CDCl_3 relative to external tetramethylsilane (TMS). Singlet peaks, each with small side bands, were observed at 7.27, 4.63, and 1.57 ppm corresponding to CHCl_3 , H_2 , and H_2O , respectively.



The ^1H NMR spectrum (2–7.5 ppm) on a sealed sample of liquid-nitrogen-condensable helium-hydrogen plasma gases dissolved in CDCl_3 relative to tetramethylsilane (TMS). A singlet peak was observed at 7.27 which matched CHCl_3 . No H_2 peak was observed at 4.63 ppm. Rather, a novel singlet peak was observed at 3.25 ppm which could not be assigned to a known compound. This upfield peak relative to H_2 was assigned to $\text{H}_2(1/p)$. An additional reproducible singlet peak was observed at 3.23 ppm that may be due to an ortho-para effect in $\text{H}_2(1/p)$ wherein the relative internuclear separation goes as $1/\rho$.



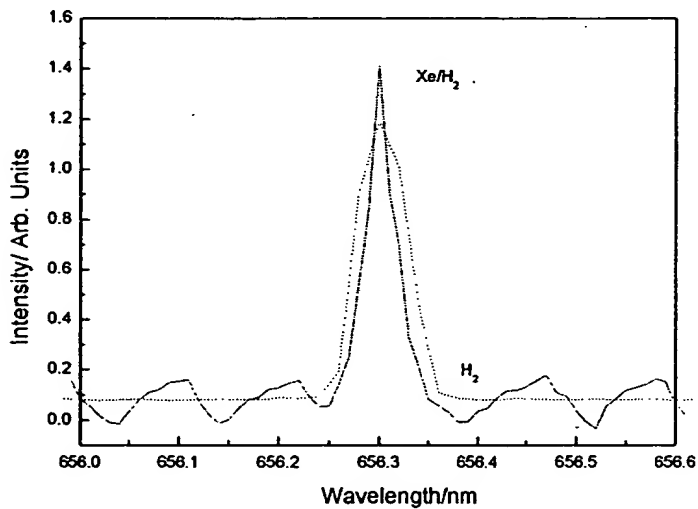
The ^1H NMR spectrum (3–8 ppm) on a sealed sample of liquid-nitrogen-condensable helium-hydrogen plasma gases dissolved in CDCl_3 relative to tetramethylsilane (TMS). A singlet peak was observed at 7.27 which matched CHCl_3 , and the H_2 peak was observed at 4.63 ppm. Novel singlet peaks were observed at 3.40 and 3.10 ppm which could not be assigned to a known compound. These upfield peaks relative to H_2 were assigned to $\text{H}_2(1/p)$.



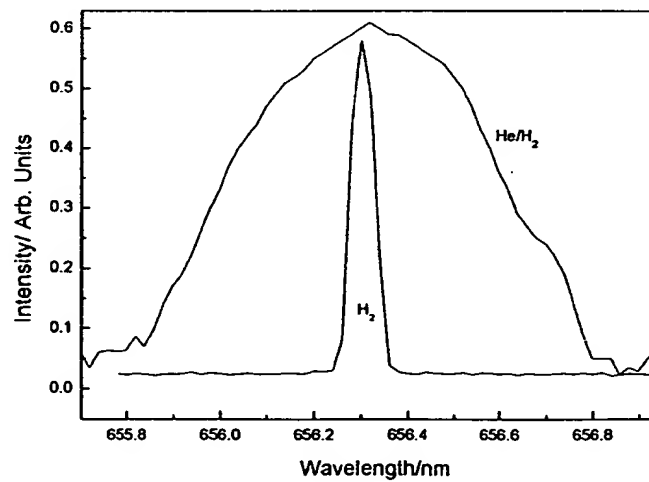
The gas chromatograph of a helium-hydrogen (60/40%) mixture before (a) and after (b) the microwave discharge which was collected in a liquid nitrogen cryotrap. It was extraordinary that ordinary hydrogen with trace helium was condensed with the major fraction of the gas that was observed with a longer retention time and was assigned to $H_2(1/\rho)$.

Exothermic Reaction Characterization

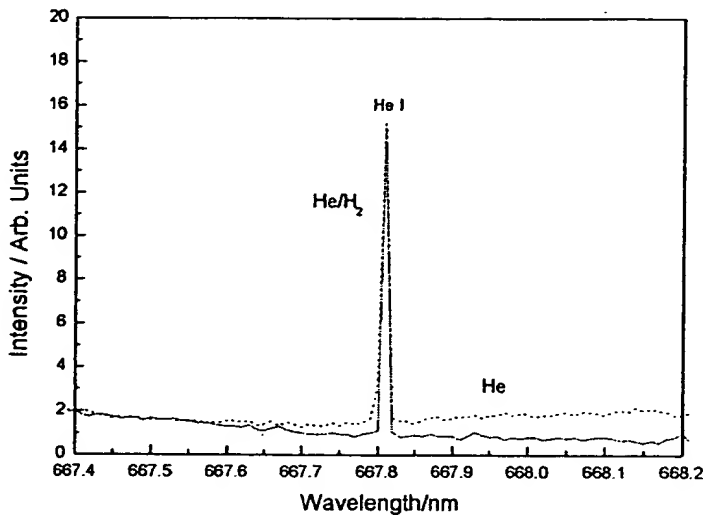
Balmer Line Broadening Calorimetry



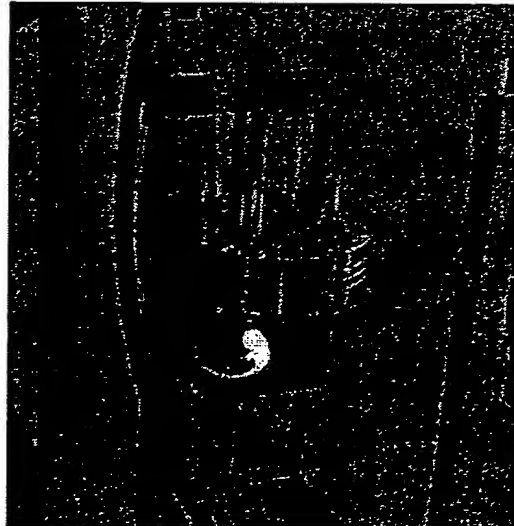
The 656.3 nm Balmer α line width recorded with a high resolution (± 0.006 nm) visible spectrometer on a xenon-hydrogen (90/10%) (solid curve) and a hydrogen microwave discharge plasma (dotted curve). No line excessive broadening was observed from either plasma corresponding to an average hydrogen atom temperature of 1–2 eV.



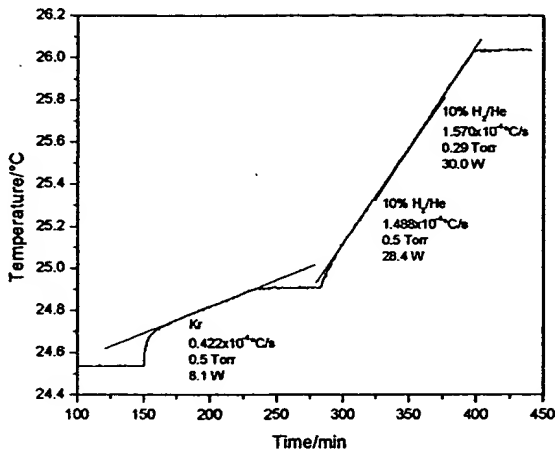
Significant broadening of Balmer α line was observed corresponding to an average hydrogen atom temperature of 180–210 eV.



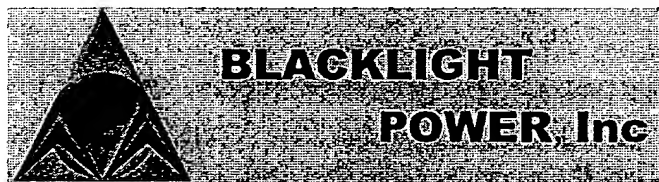
The 667.816 nm He I line width recorded with a high resolution (± 0.006 nm) visible spectrometer on helium-hydrogen (90/10%) (solid curve) and helium (dotted curve) microwave discharge plasmas. No broadening was observed in either case.



Plasma cell that is immersed in water bath calorimeter



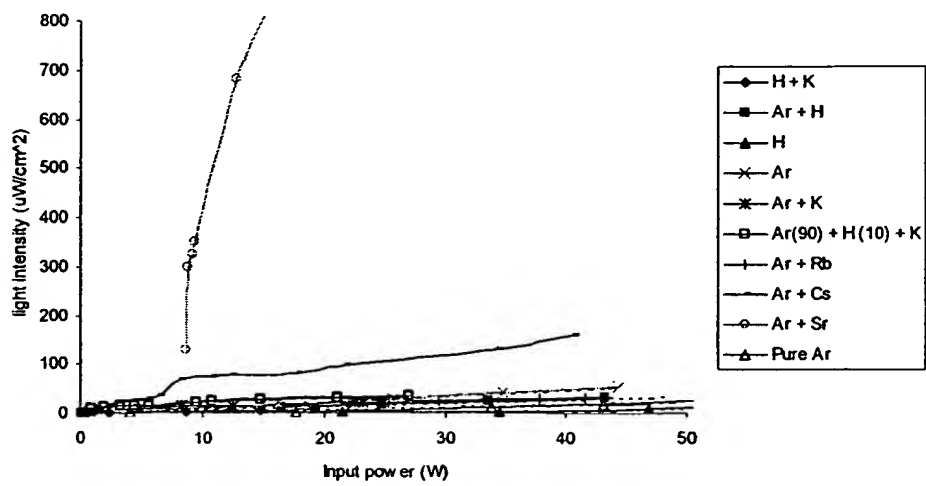
The $T(t)$ water bath response to stirring and then with selected panel meter readings of the constant forward and reflected microwave input power to krypton was recorded. The microwave input power was determined to be 8.1 ± 1 W. A helium-hydrogen (90/10%) mixture was run at identical microwave input power readings as the control, and the excess power was determined to be 21.9 ± 1 W from the $T(t)$ response.



Catalyst Comparison For Optical Power Balance

8,600 Times Less Power Required to Achieve the Same Light Emission with Strontium-Argon Catalyst Present Compared to Control

Comparison of input power vs. light intensity for different gasses & catalysts



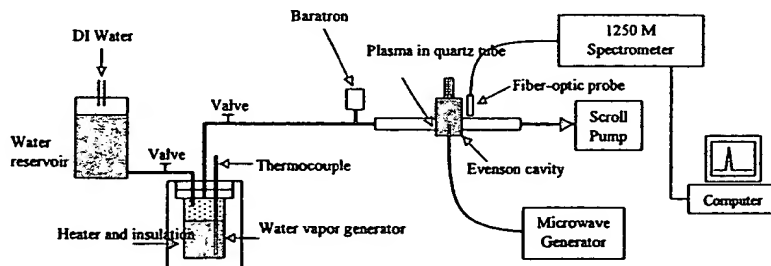
Discharge conditions and comparison of the driving power to achieve a total visible radiant flux of about $1\mu\text{W}/\text{cm}^2$

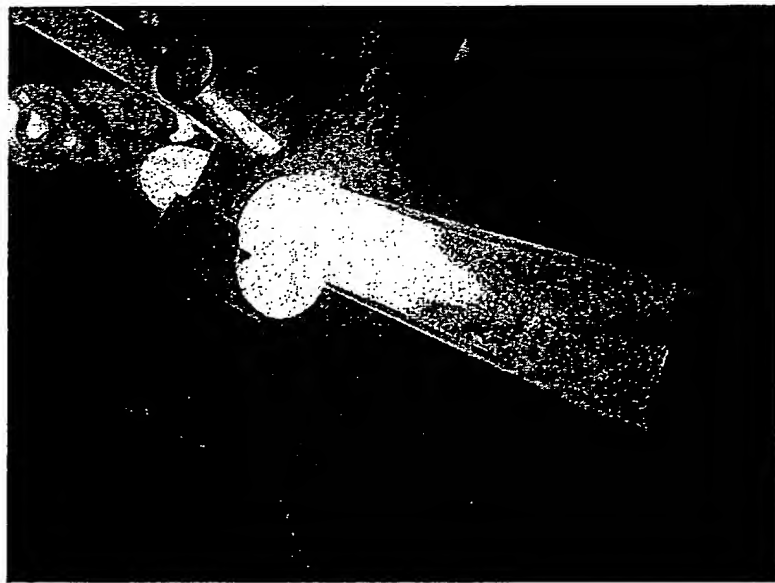
	T (°C)	P _{hyd.} (torr)	P _{Ar} (torr)	P _v (torr) ^a	Voltage (V)	Current (mA)	Integ. time (ms)	Detector irradiation ($\mu\text{W}/\text{cm}^2$)	Power (W)
Ar+H ₂ +Sr	514	0.3	1.0	0.006	6.56	0.6	204	1.3	0.0039
Ar+H ₂	519	0.295	0.5	—	224	184	409	1.9	33.5 ^b
Ar	520	—	1.0	—	190	170	307	1.1	24.7 ^b
H ₂ +Sr	664	—	—	0.270	2.20	3.86	768	1.17	0.0085
H ₂	664	1.0	—	—	224	110	1130	2.08	24.6
H ₂ +Na	335	1.0	—	0.051	272	124	122	1.85	33.7
H ₂ +Na	516	1.5	—	5.3	220	68	768	0.40	15.0
H ₂ +Na	664	1.5	—	63	240	41	768	0.41	9.84
H ₂ +Mg	449	4.0	—	0.016	153	380	500	1.7	58
H ₂ +Mg	582	4.2	—	0.6	233	290	500	0.16	68
H ₂ +Mg	654	3.0	—	2.8	250	400	1000	0.18	100.0
H ₂ +Ba	666	2.0	—	0.025	138	730	716	0.03	55 ^b
Bkgnd.	664	—	—	0.270	0	0	768	0.20	0

^a Calculated.

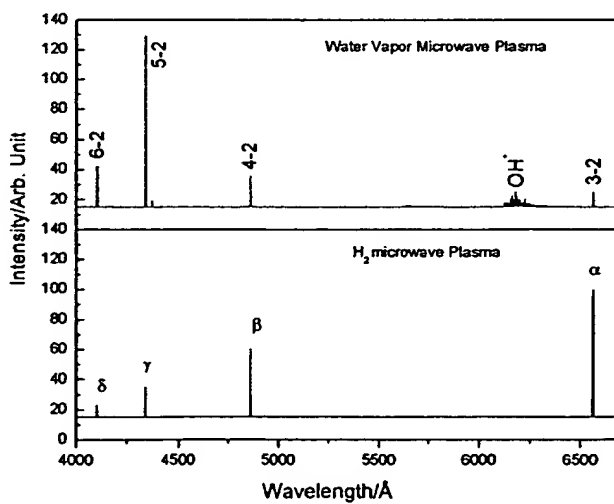
^b Power input differs from volt-amperes due to non-unity power factor.

Experimental Set-up for Water Microwave Plasma

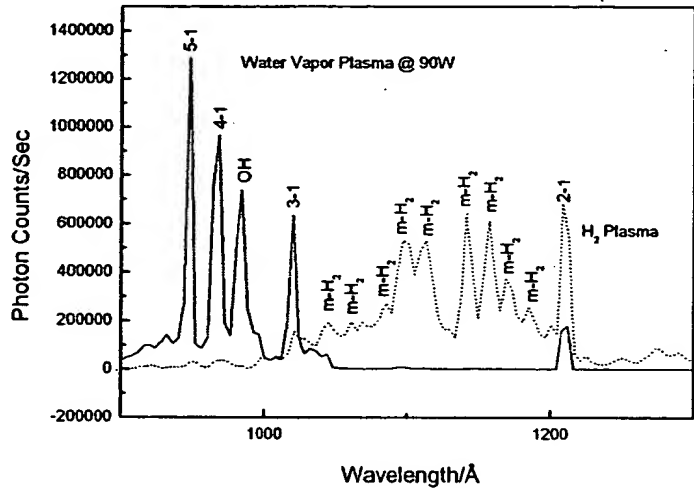




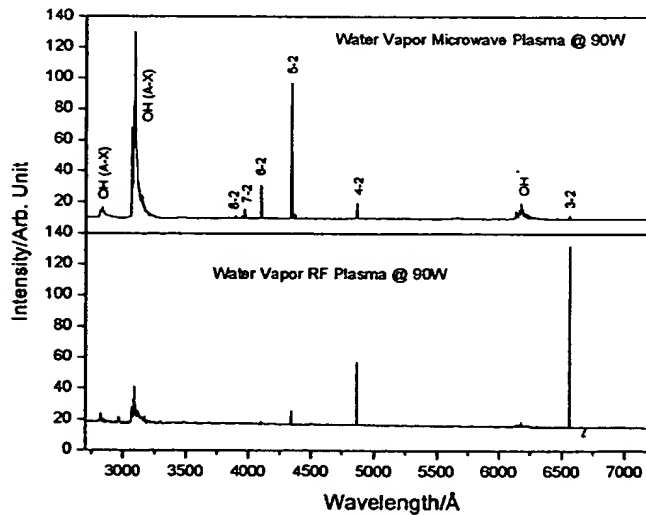
Water Vapor Plasma



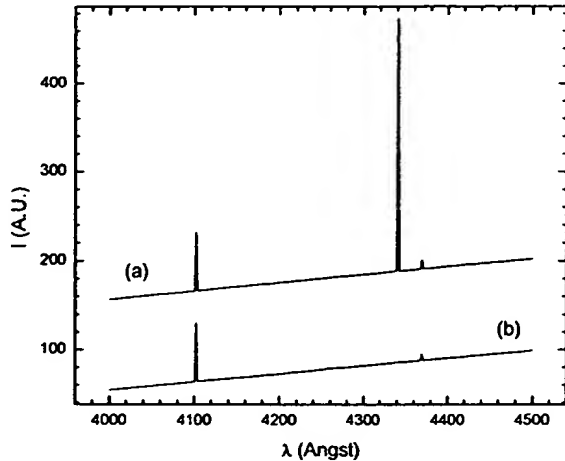
The visible spectra (4000–6700 Å) of the cell emission from a water microwave plasma with 90 W input power (top) and a hydrogen microwave plasma at 90 W input power (bottom). A stationary inverted H Balmer population was observed from the low pressure water-vapor microwave discharge plasma. The population of the level $n = 4, 5$, and 6 of hydrogen was continuously inverted with respect to $n = 3$ and the $n = 5$, and 6 levels were further continuously inverted with respect to $n = 4$.



The VUV spectra (900–1300 Å) of the cell emission from hydrogen microwave (dotted line) and the water microwave (solid line) plasmas with 90 W input power. An inverted Lyman population was observed from the water plasma emission with the inversion observed in the visible as shown in previous figure extending to the $n = 2$ level.



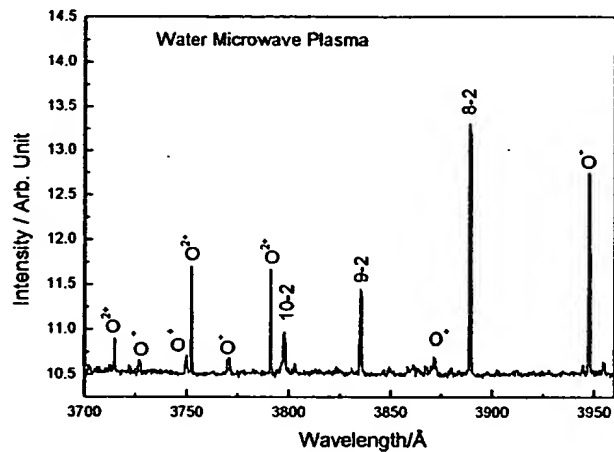
The visible spectra (2800–7200 Å) of the cell emission from water microwave (top) and inductively coupled RF (bottom) plasmas with 90 W input power. The population of the levels $n = 4, 5, 6, 7, 8$, and 9 of hydrogen was continuously inverted with respect to $n = 3$ in the water microwave plasma; whereas, no inversion was observed in the RF plasma.



The results of back illumination with a 70 W incandescent lamp where (a) is the sum of the independent lamp and plasma spectra and (b) the spectrum recorded with the lamp and plasma run simultaneously. Background (dark) spectra were subtracted from both traces shown. Spectrum (a) has been shifted upward by 100 A.U. for illustration purposes. The absence of the Balmer γ 4340 Å line corresponding to the $n=5$ to $n=2$ transition indicates that the lamp stimulated the depopulation of the $n=5$ state to one or more of the $n=4$ and $n=3$ states.

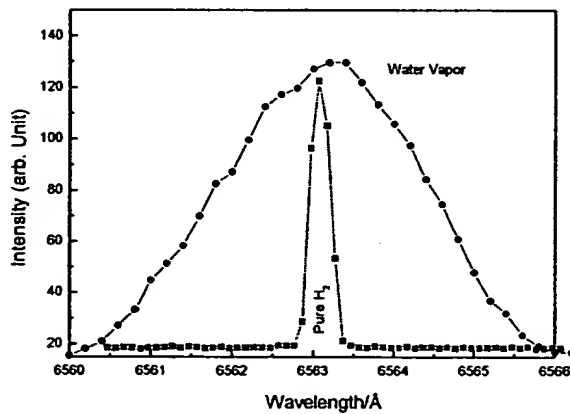
Potential laser transitions of atomic hydrogen in a microwave water-vapor plasma

Wavelength/Å	Spectral Region	Electronic Transition
		$n_{\text{initial}} - n_{\text{final}}$
74,578	IR	$6 \rightarrow 5$
40,512	IR	$5 \rightarrow 4$
26,252	IR	$6 \rightarrow 4$
18,751	IR	$4 \rightarrow 3$
12,818	IR	$5 \rightarrow 3$
10,938	IR	$6 \rightarrow 3$
10,049	IR	$7 \rightarrow 3$
6,563	red	$3 \rightarrow 2$
4,861	blue	$4 \rightarrow 2$
4,340	violet	$5 \rightarrow 2$
4,102	violet	$6 \rightarrow 2$
3,970	violet	$7 \rightarrow 2$
3,889	violet	$8 \rightarrow 2$



The visible spectrum (3700–3960 Å) of the cell emission from a water microwave plasma at 90 W input power. The catalysis mechanism was supported by the observation of O²⁺ at 3715.0 Å, 3754.8 Å, and 3791.28 Å. O⁺ was observed at 3727.2 Å, 3749.4 Å, 3771 Å, 3872 Å, and 3946.3 Å. The hydrogen Balmer lines corresponding to the transitions 10–2, 9–2, and 8–2 were also observed.

Balmer α -Line Broadening

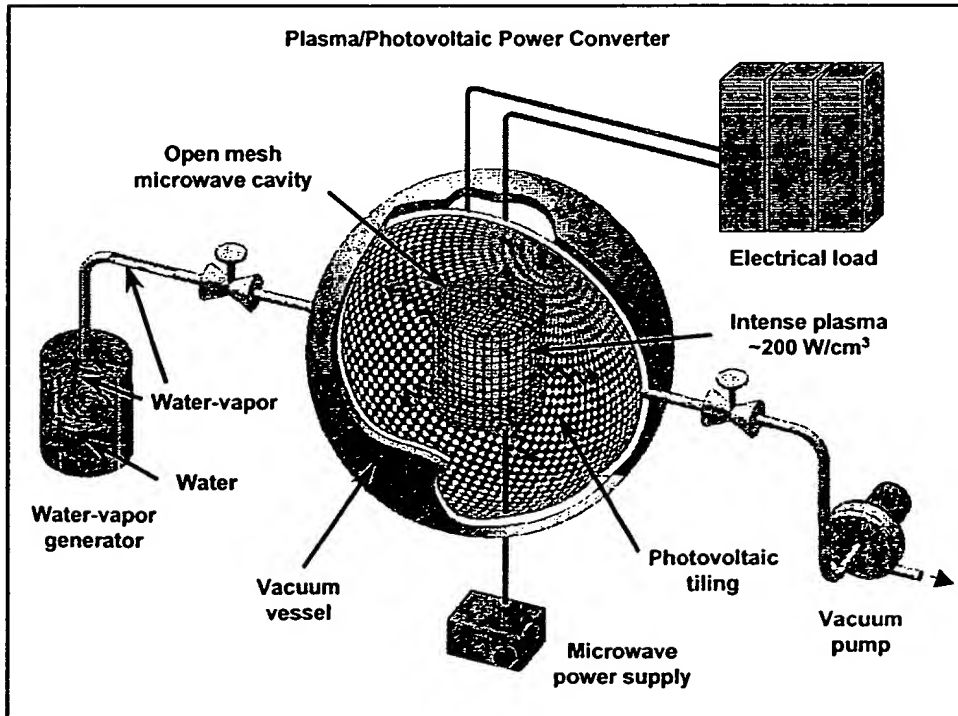


The 6562.8 Å Balmer α -line width recorded with a high resolution (± 0.06 Å) visible spectrometer on a hydrogen microwave plasma.

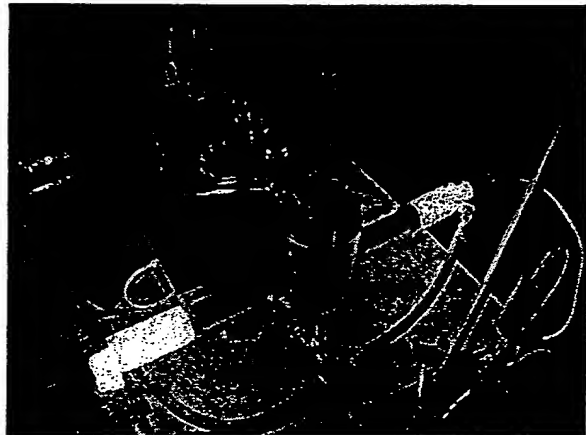
The pumping rate and pumping power calculated from the collisional-radiative model for laser transitions 5-2, 5-3, and 6-2

Laser Transition	Calculated Pumping Rate of Upper Level ($10^{19} \text{ cm}^3 \text{s}^{-1}$)	Calculated Pumping Power ($\text{W} \cdot \text{cm}^3$)
5-2	8.4 ^a	175.3 ^a
5-3		
6-2	2.12	44.8

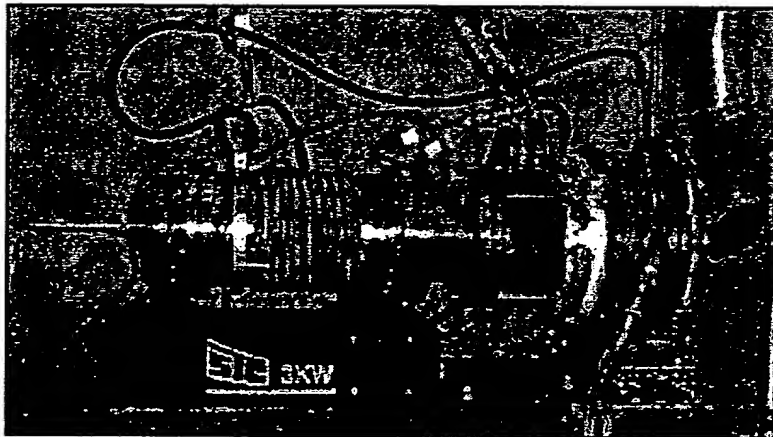
^a for 5-2 and 5-3 transitions

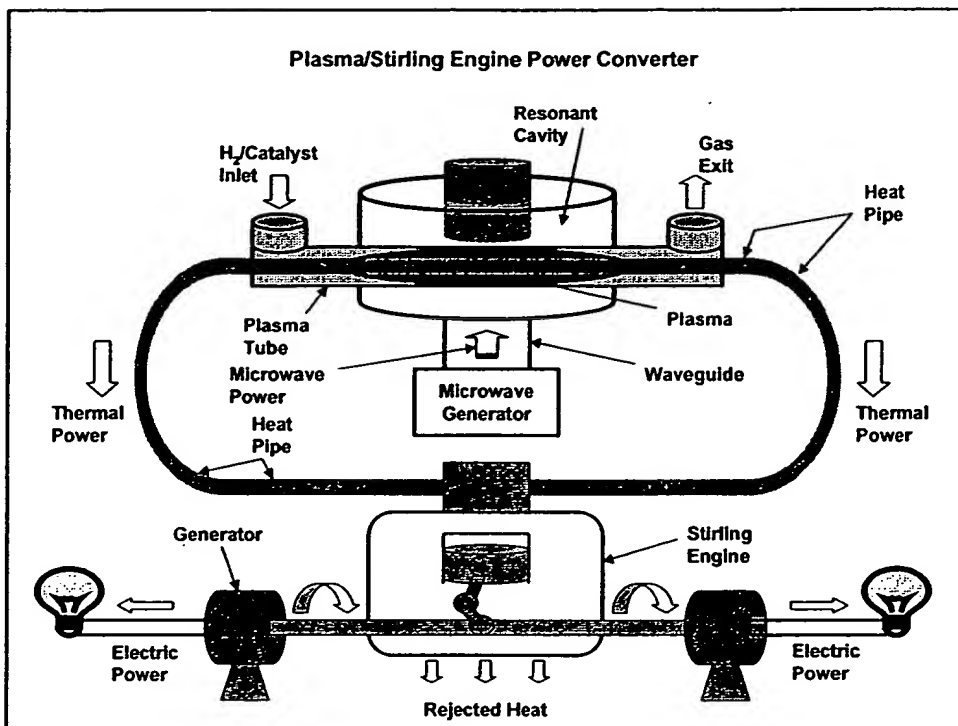


Plasma Power Scale-Up



3 kWe Stirling Engine
STC Inc.





Major Components Cost Estimate for Mass-Produced BLP Electric Generator

Component Costs (Direct)	Dollars
Photovoltaic Array	25 per kW
Inverter, control, wires	50 per kW
Cooling	5 per kW
Balance of Plant (independent of size)	282

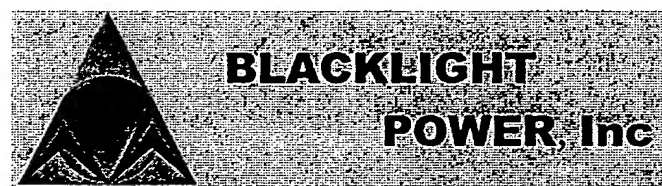
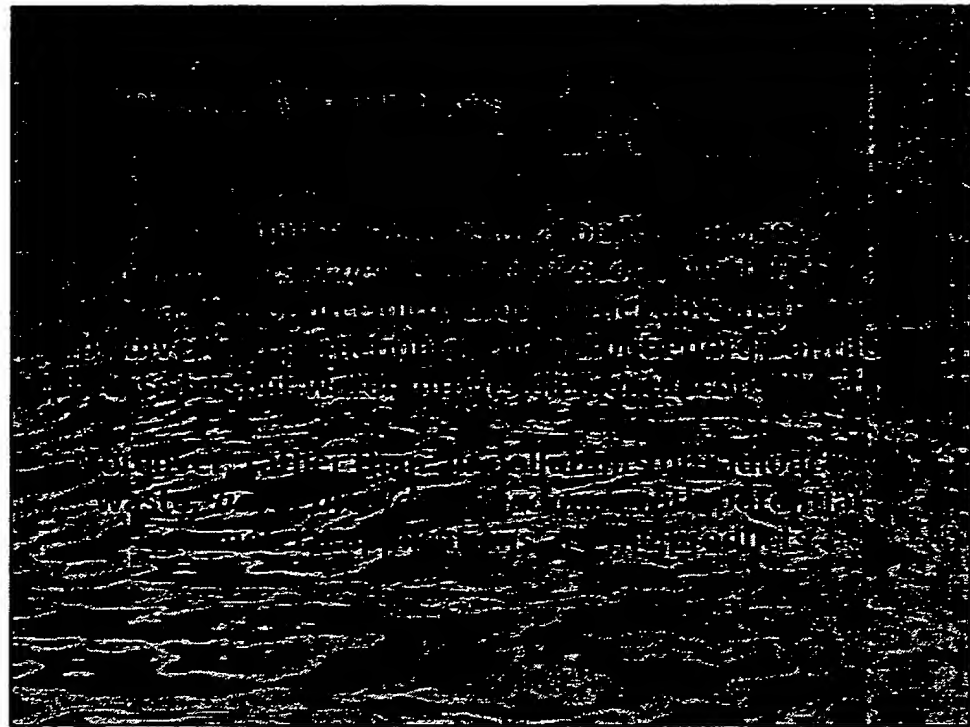
Unit Costs: BLP vs Competitors

Technology Type	Average Generating Capacity (kW)	Power Density (W/cm ²)	Fuel Volumetric Energy Density (kWh/gal)	Fuel Mass Energy Density (kWh/kg)	Installed Cost (\$/kW)	Fuel Cost (\$/kW h)
BLP Energy Technology	25	40	23,000	6,000	150	0
PEM Fuel Cell	25	1	9	33	3,700**	0.065
Internal Combustion Engine	100	40	33	12	1,400**	0.044
Industrial Gas Turbine	1000	1	19	12	1,600	0.038
Natural Gas Microturbine	100	1	19	12	2,000	0.044
Photovoltaic	10	0.01*	N/A	N/A	8,000	0
Coal	400,000	0.3	N/A	8.3	1,100	0.015
Nuclear	600,000	2	N/A	N/A	2,200	0.006

Source: DOE, EPRI, ENREN *Watts per square centimeter **Current Cost of stationary distributed generation equipment

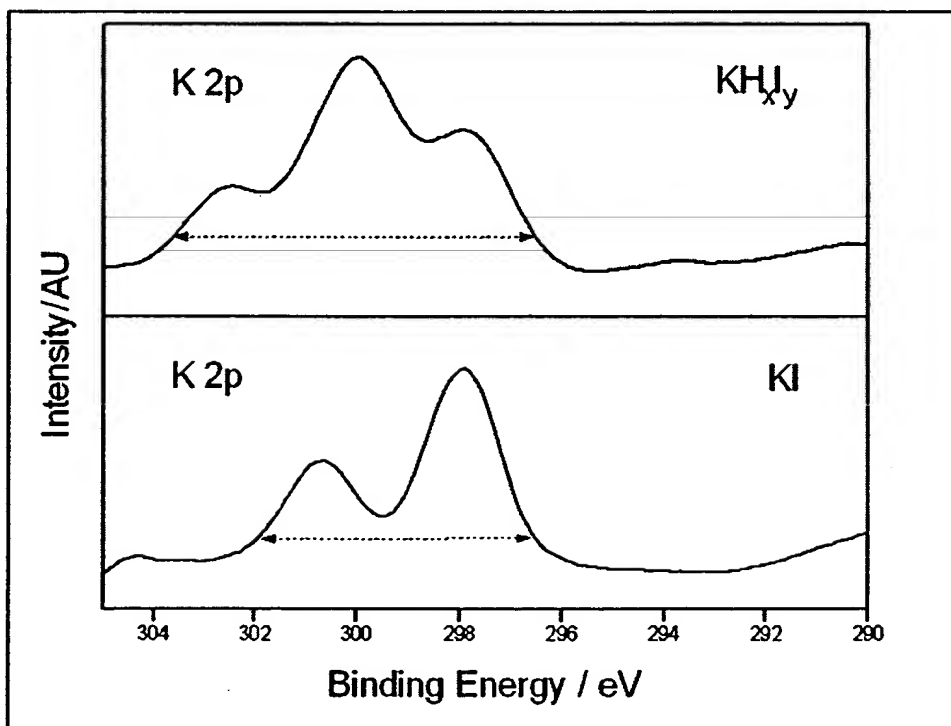
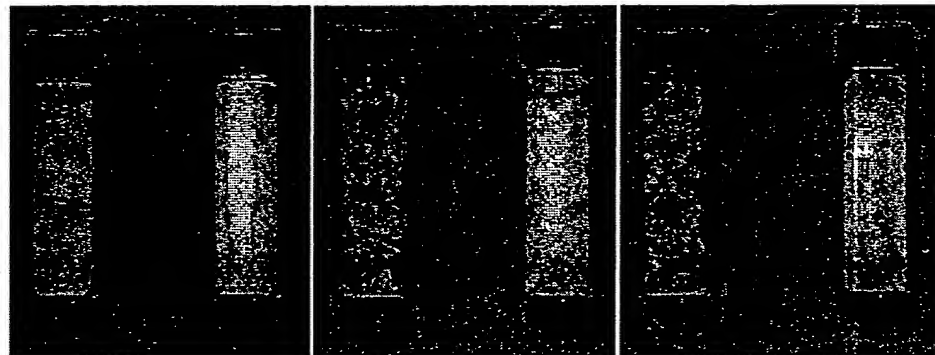
BLP MicroGen Advantages

- No Fuel Costs
- Solid State Device
- Cost Competitive (Lower Capital and O&M Costs)
- No Fuel Handling Issues / Pollution
- Load Following
- No Grid Connection (Gas or Electric for Fuel or Load Leveling)
- Valuable chemical products

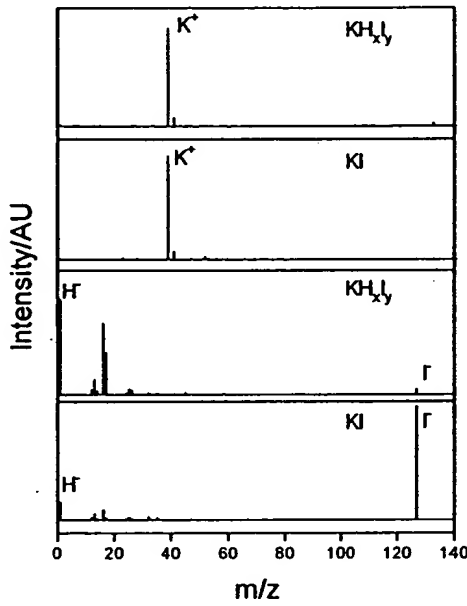


Novel Hydride Compounds

Novel Hydride Compounds



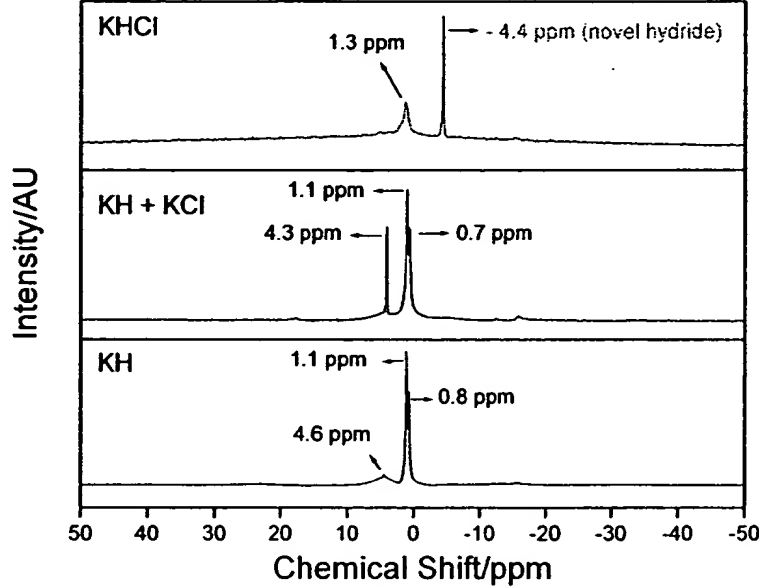
Hydride Compound (H-)



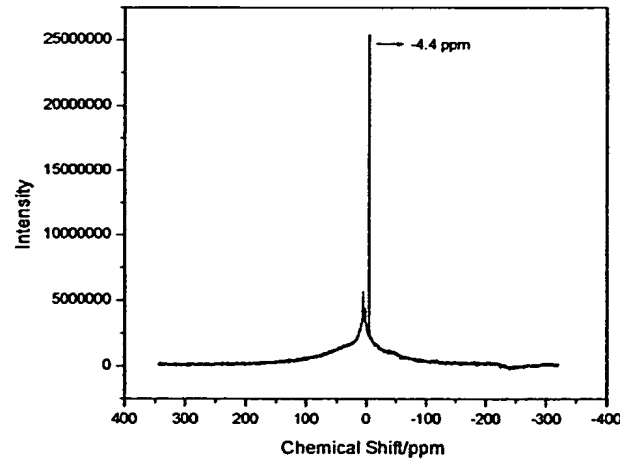
Solid-State MAS $^1\text{H-NMR}$

- Chemical environment of hydrogen
- Unusual upfield shifts – relative to normal hydride

(the electron is closer to the nucleus in a smaller hydride ion called a hydrino hydride ion)



Upfield-shifted NMR peak demonstrates novel hydride.



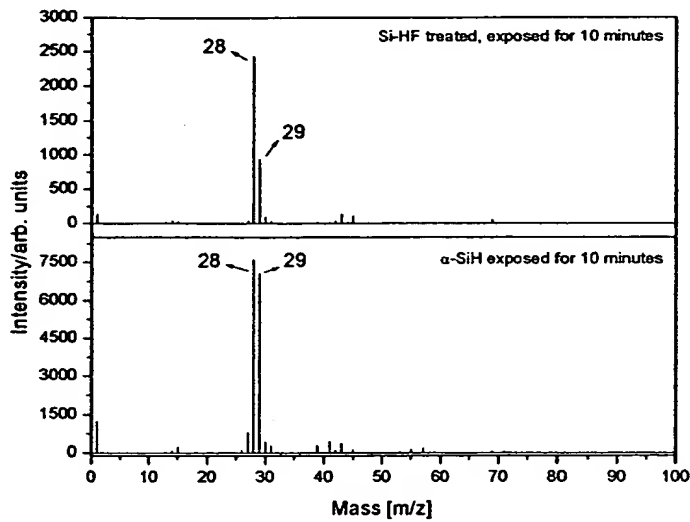
The ^1H MAS NMR spectrum (-300 to +300 ppm) relative to external tetramethylsilane (TMS). The novel upfield resonance at -4.4 relative to TMS corresponding to an absolute resonance shift of -35.9 ppm matched the theoretical prediction of $\rho = 4$ and identified the $\text{H}'(1/4)$ hydride ion of $\text{KH}'\text{Cl}$.

Potential Applications

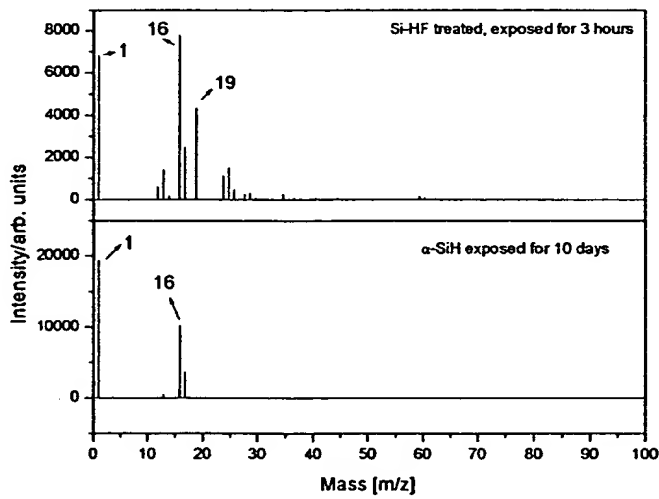
- Chemical products and processes based on hydrino-silicon chemistry, such as:
 - hydrino-terminated silicon for chip fabrication
 - amorphous hydrino-silicon for photovoltaics
 - hydrino silane as precursors
 - hydrino etching and doping processes;
- Synthesis of single crystal diamond films;
- Metal hydrides such as AuH and FeH which do not corrode to be used as anticorrosive coatings, cladding, stealth, and heat and chemical resistance;
- Light-weight, high-strength structural materials for ships and air frames;
- Ferromagnetic conductive plastics for magnetic shielding (μ -materials) in applications such as fiber optics and television tubes, storage media, generators, electric motors, sensors, actuators, computer, and electronics packaging.

Hydrino-Terminated Amorphous Silicon

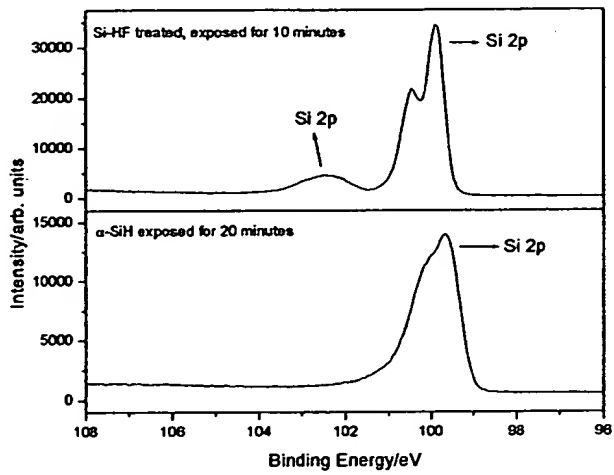
- Highly Stable in Air
- Formed by Plasma Process
- Could Eliminate HF Wet Chemistry Step
- Could Increase Chip Yield and Decrease
- Production Time
- Could Enhance Device Performance



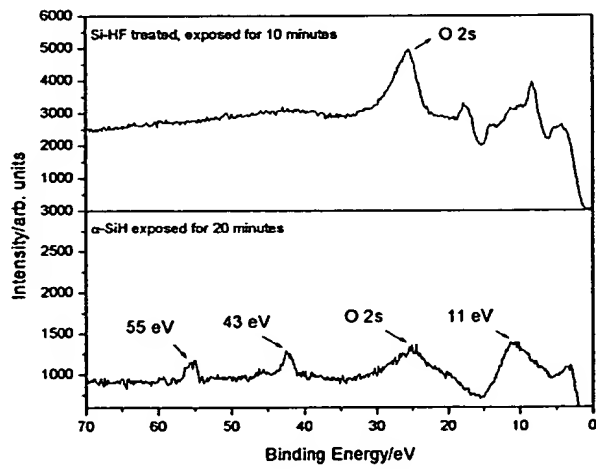
The positive ion ToF-SIMS spectra ($m/e=0-100$) of the HF cleaned silicon wafer exposed to air for 10 min. before ToF-SIMS analysis (top), and a nickel foil coated with an α -SiH film and exposed to air for 10 min. that showed a large SiH^+ peak (bottom).



The negative ion ToF-SIMS spectra ($m/e=0-100$) of HF cleaned silicon wafer exposed to air for 3 hours before ToF-SIMS analysis showing a dominant oxide peak (top), and a nickel foil coated with an α -SiH film and exposed to air for 10 days before the ToF-SIMS analysis that retained the dominant hydride ion peak (bottom).



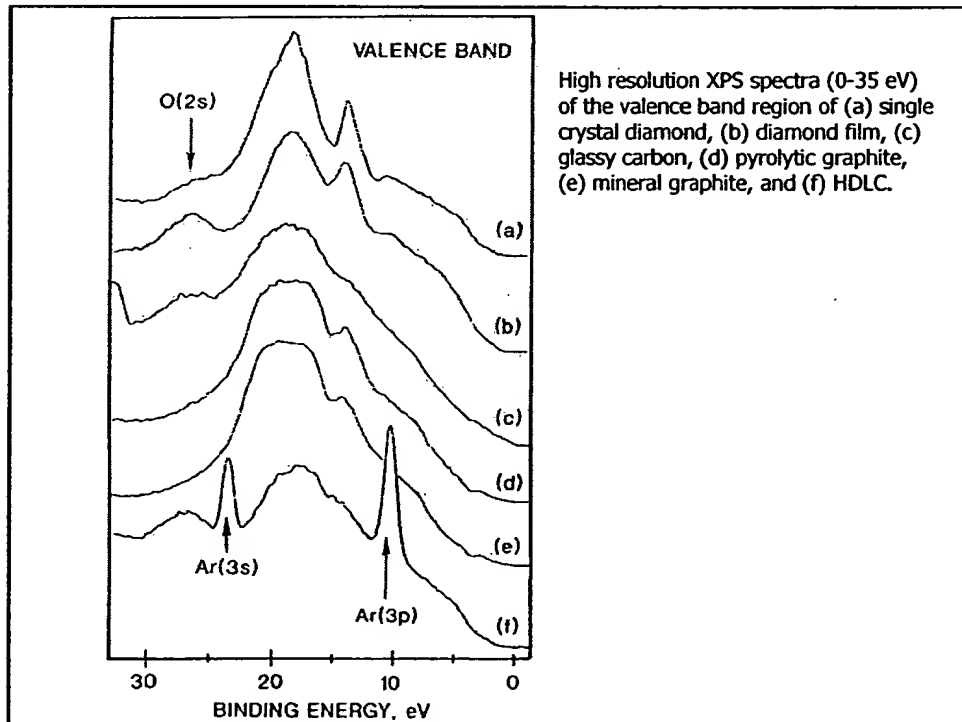
The XPS spectra (96–108 eV) in the region of the $Si\ 2p$ peak of the HF cleaned silicon wafer exposed to air for 10 min. before XPS analysis showing a very large SiO_x peak in the region of 101.5–104 eV (top), and a nickel foil coated with an α - SiH film and exposed to air for 20 min. before XPS analysis showing no oxide in the region of 104 eV (bottom).

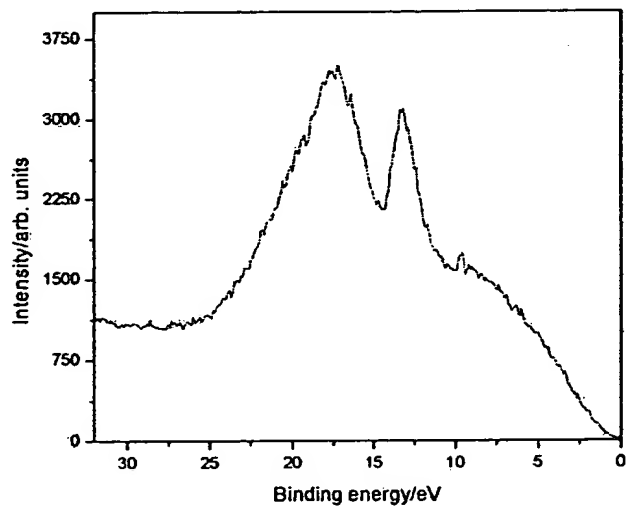


The 0–70 eV binding energy region of a high resolution XPS spectrum of the HF cleaned silicon wafer exposed to air for 10 min. before XPS analysis showing only a large $O\ 2s$ peak in the low binding energy region (top), and a nickel foil coated with an α - SiH film and exposed to air for 20 min. before XPS analysis (bottom). The novel peaks observed at 11, 43 and 55 eV which could not be assigned to the elements identified by their primary XPS peaks matched and were assigned to $H(1/4)$, $H(1/9)$, and $H(1/11)$. The novel highly stable hydride ions formed by the catalytic reaction of He^+ and atomic hydrogen may be the basis of the extraordinary stability of the α - SiH film.

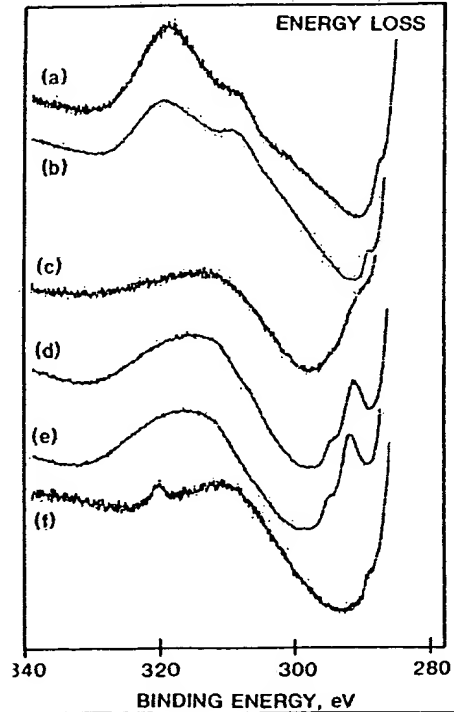
Single Crystal Diamond

- High Deposition (20 microns/hr)
- Low Substrate Temperature (Room Temperature Possible)
- Unique Energetic Plasma
- Solid Carbon or Methane Reactant
- Without Diamond Seeding
- Very Low Power - 40 W

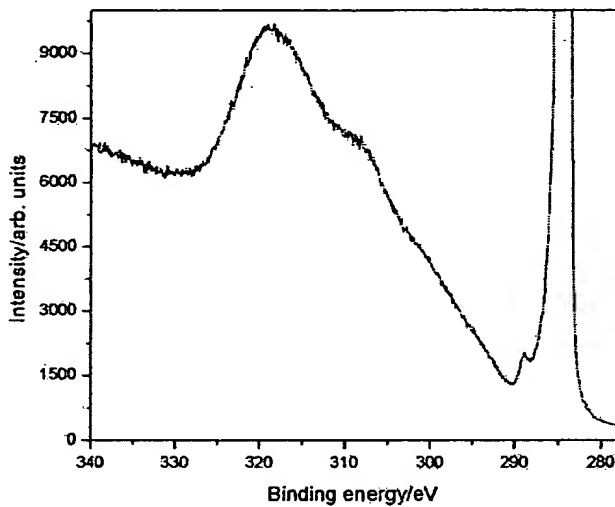




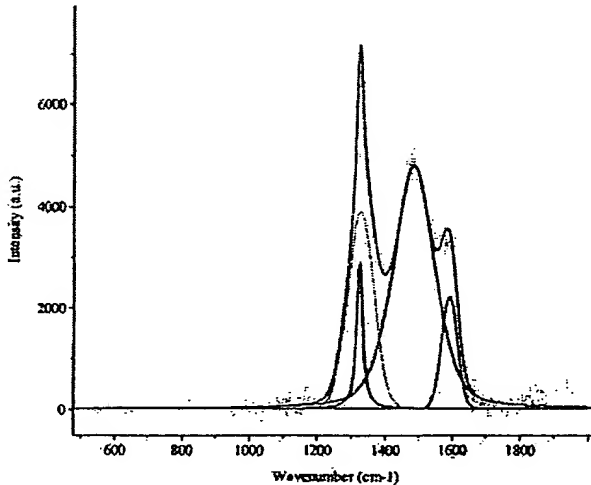
High resolution XPS spectra (0-35 eV) of the valence band region of a cleaned commercial silicon wafer coated by reaction of a helium-hydrogen plasma with CH_4 as the source of C that showed features that matched single crystal diamond.



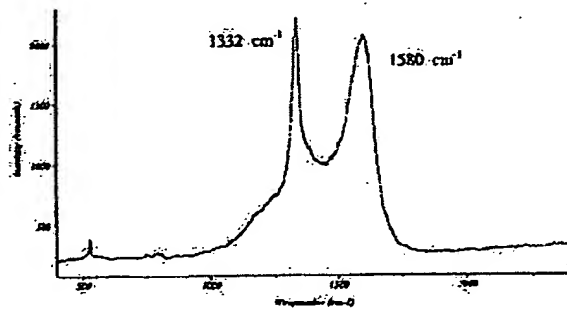
High resolution XPS spectra (280-340 eV) of the C1s energy loss region of (a) single crystal diamond, (b) diamond film, (c) glassy carbon, (d) pyrolytic graphite, (e) mineral graphite, and (f) HDLC.



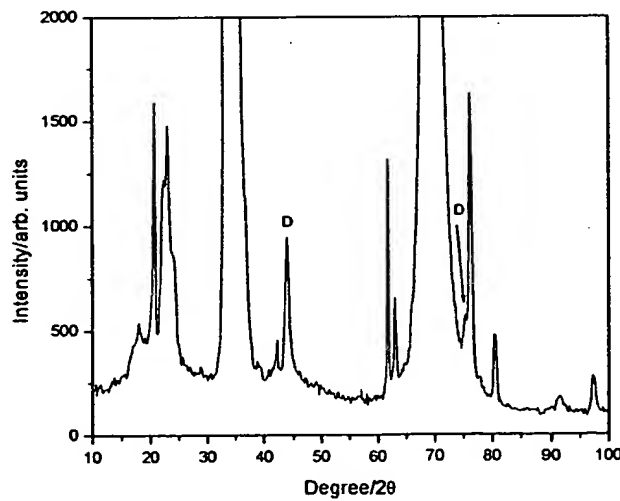
High resolution XPS spectrum (280-340 eV) of the C 1s energy loss region of a cleaned commercial silicon wafer coated by reaction of a helium-hydrogen plasma with CH_4 as the source of C that showed features that matched single crystal diamond.



The Raman spectrum recorded on the diamond film. The diamond band, D-band, G-band of DLC, and G-band of graphite were observed at 1323.5 cm^{-1} , 1327.0 cm^{-1} , 1484.0 cm^{-1} and 1591.6 cm^{-1} , respectively. The 19.6 cm^{-1} FWHM of the diamond peak is characteristic of and identified the film as having single crystal diamond.



The Raman spectrum of a second diamond film formed by helium-hydrogen-methane (48.2/48.2/3.6%) microwave discharge plasma CVD. A diamond band was observed at 1332 cm^{-1} . In addition, the G-band of graphite was observed at 1580.



The X-ray Diffraction (XRD) pattern of a diamond film for $2\theta = 10^\circ$ to 100° . The dominant peaks were due to silicon of the substrate. Diamond peaks (D) were observed at $2\theta = 43.9^\circ$ (111) and 75.3° (220).

Acknowledgements



**Bala Dhandapani, Director, Chemical Synthesis
and Analysis**

Ph.D. Chemical Engineering—Clarkson University, Potsdam, NY



Mark Nansteel, Director, Plasma Cell Engineering

Ph.D. Mechanical Engineering—University of California, Berkeley



Bob Mayo, Director, Plasma-to-Electric Conversion

Ph.D. Nuclear Engineering—Purdue University



Paresh Ray, Research Scientist

Ph.D. Physical Chemistry - Indian Institute of Science

Post Doc- University of Chicago

Post Doc- Columbia University



www.blacklightpower.com

**This Page is Inserted by IFW Indexing and Scanning
Operations and is not part of the Official Record**

BEST AVAILABLE IMAGES

Defective images within this document are accurate representations of the original documents submitted by the applicant.

Defects in the images include but are not limited to the items checked:

- BLACK BORDERS**
- IMAGE CUT OFF AT TOP, BOTTOM OR SIDES**
- FADED TEXT OR DRAWING**
- BLURRED OR ILLEGIBLE TEXT OR DRAWING**
- SKEWED/SLANTED IMAGES**
- COLOR OR BLACK AND WHITE PHOTOGRAPHS**
- GRAY SCALE DOCUMENTS**
- LINES OR MARKS ON ORIGINAL DOCUMENT**
- REFERENCE(S) OR EXHIBIT(S) SUBMITTED ARE POOR QUALITY**
- OTHER:** _____

IMAGES ARE BEST AVAILABLE COPY.

As rescanning these documents will not correct the image problems checked, please do not report these problems to the IFW Image Problem Mailbox.

THIS PAGE BLANK (USPTO)